APL Photonics ARTICLE scitation.org/journal/app

Computational Doppler-limited dual-comb spectroscopy with a free-running all-fiber laser

Cite as: APL Photon. 4, 116102 (2019); doi: 10.1063/1.5117847
Submitted: 1 July 2019 • Accepted: 22 October 2019 •
Published Online: 11 November 2019

Łukasz A. Sterczewski,[1] Aleksandra Przewłoka,[2] Wawrzyniec Kaszub,[2] and Jarosław Sotor[1,a)]

AFFILIATIONS

[1] Laser & Fiber Electronics Group, Faculty of Electronics, Wroclaw University of Science and Technology, Wybrzeze Wyspianskiego 27, 50-370 Wroclaw, Poland
[2] Institute of Electronic Materials Technology, Wolczynska 133, 01-919 Warsaw, Poland

[a)] **Author to whom correspondence should be addressed:** jaroslaw.sotor@pwr.edu.pl.

ABSTRACT

Dual-comb spectroscopy has emerged as an indispensable analytical technique in applications that require high resolution and broadband coverage within short acquisition times. Its experimental realization, however, remains hampered by intricate experimental setups with large power consumption. Here, we demonstrate an ultrasimple free-running dual-comb spectrometer realized in a single all-fiber cavity suitable for the most demanding Doppler-limited measurements. Our dual-comb laser utilizes just a few basic fiber components, allows us to tailor the repetition rate difference, and requires only 350 mW of electrical power for sustained operation over a dozen of hours. As a demonstration, we measure low-pressure hydrogen cyanide within 1.7 THz bandwidth and obtain better than 1% transmittance precision over a terahertz in 200 ms enabled by an all-computational phase retrieval and correction algorithm. The combination of the setup simplicity, comb tooth resolution, and high spectroscopic precision paves the way for proliferation of frequency comb spectroscopy on a larger scale.

INTRODUCTION

Molecular spectroscopy with optical frequency combs (OFCs)[1] has experienced a remarkable growth in the last decade propelled by the brilliant concept of the simultaneously broadband and discrete nature of the light source, allowing to merge high-resolution laser spectroscopy with broadband spectral coverage. The relentless pursuit for precision[2] drove the scientific community to progressively turn initially free-running mode-locked lasers into precise frequency rulers[3–7] referenced to atomic clocks with relevance for astrophysics studies.[8]

New avenues for OFC-based spectroscopy have been opened with the inception of the dual-comb spectroscopy (DCS) technique[9–11] employing optical beating between two repetition rate mismatched frequency combs on a photodetector, which quickly surpassed the speed and precision of conventional Fourier Transform Spectroscopy (FTS). The novel all-solid-state spectroscopic technique paved the way for a highly miniaturized real-time optical spectrum analyzer that multiheterodynes a discrete comb teeth to establish a direct link between the optical and radio frequency (RF) domains, permitting acquisition times ranging from micro- to milliseconds. In past few years, a surge of activity in the development of chip-scale dual-comb systems provided compact DCS platforms based on microresonators,[12–14] quantum cascade,[15,16] and interband cascade lasers,[17] which hold promise for a portable, field-deployable spectroscopic sensor covering different spectral regions.

Unfortunately, the convenience of DCS has its price. A majority of dual-comb spectrometers rely on two synchronized OFCs using complex phase locking loops necessitating the use of additional single-mode lasers, photodetectors, and fast control electronics.[5] Otherwise, substantial amounts of phase noise arising from the unsynchronized operation of two free-running oscillators smear out the discrete character of the RF lines, hence precluding reliable spectroscopic assessments. To circumvent this issue, a well-known noise suppression technique can be employed, conceptually similar to balanced transmission widely used in electrical engineering, because in DCS, a critical requirement is mutual rather than absolute stability. By generating two combs in a single cavity, most of the environmental perturbations causing phase-noisy operation of the combs become common; hence, such combs show a much higher degree of

mutual coherence than a pair generated in two independent cavities. While their absolute frequency remains unstabilized, from a practical standpoint optical frequency drifts occurring on time scales suitable for spectroscopy with a (sub)percentage level of uncertainty are much lower than molecular Doppler linewidths, which makes them compatible even with demanding high-resolution applications.

The burgeoning field of single-cavity dual-comb (SCDC) lasers is constantly being enriched with new concepts. To date, the most popular fiber-based SCDC generation mechanisms employ bidirectional mode-locking of a ring cavity,[18–21] dual-wavelength lasing,[22–27] and nonlinear pulse shaping mechanisms.[28] Their full spectroscopic potential, however, has been weakly exploited to date. A vast majority reported on measurements at atmospheric pressure with apodized spectra, where gigahertz resolution is more than sufficient, while their repetition rates were relatively low—they ranged between a dozen and several dozen megahertz. To date, such DCS systems have been perceived as suitable only for coarse spectroscopic investigations.[5] A notable exception from the above was provided by Zhao *et al.*, who demonstrated picometer resolution measurements of acetylene using an all-fiber dual-color mode-locked laser.[22] The experiment, however, employed nonlinear broadening mechanisms relying on a chain of optical components and pumping diodes for optical amplification of spectrally filtered subcombs, which adds an extra layer of complexity and makes it difficult to meet tight power budget constraints. Similar issues arise in a rivaling electro-optic (EOM) comb generation technique, which despite the repetition rate agility and ease of optical frequency axis calibration[29] also require nonlinear broadening following complex microwave electro-optic circuits for competitive spectral coverage.[30]

In our work, we show that by employing polarization multiplexing[31–34] in a highly simplified all-fiber single-cavity dual-comb laser (AFSCDCL) composed of just a few basic fiber components, one can perform high-resolution broadband molecular spectroscopy with tooth-resolved rf lines using a completely free-running system characterized by low power consumption and compact size. To our knowledge, this is the simplest configuration for all-fiber dual-comb generation presented to date because two collinearly overlapping pulse trains with different repetition rates and high degrees of mutual coherence are directly accessible from the tap of the output coupler without any additional optical or electronic components. Our demonstration shows that high-resolution dual-comb spectroscopy can be simple, cost efficient, and compatible with battery operation. Except for the custom-processed graphene-based saturable absorber (GSA),[35] all components of the system have off-the-shelf commercial availability. A signature feature of our solution is that the generated combs have smooth soliton spectral shapes with almost perfect overlap; hence, they do not need any further power-hungry nonlinear broadening mechanisms and spectral filtering to avoid aliasing.[22] Furthermore, the combs' high repetition rates (>140 MHz) are tailored for molecular spectroscopy at low pressure[36] which allows for near-optimal use of optical power per comb tooth. Also, the repetition rate difference is easily tailorable from hundreds of hertz to multikilohertz (and even more) by adjusting the intracavity polarization state and by varying the length of a piece of polarization-maintaining fiber (PMF). This agility sets it apart from the bidirectional or dual-wavelength configuration, which have weakly tunable repetition rate differences defined by the bidirectional asymmetry of the cavity, and dispersive properties of the fiber, respectively. The accessible spectral range of our system exceeds 1.7 THz within 200 ms of coherent averaging, corresponding to the largest number (>11 000) of self-corrected lines relying on purely computational phase retrieval and correction. We prove the high-resolution spectroscopy capabilities of our system on a NIST standard reference material of low-pressure hydrogen cyanide $H^{13}C^{14}N$, which we measure in the $2\nu_3$ overtone band around 1.56 μm in more than 1 THz bandwidth enabled by leveraging a nontrivial computational phase correction algorithm addressing the previous issues of large computational complexity[37,38] with a potential for DCS-platform-independent character.[39] Finally, our single-cavity DCS system itself has been proven to operate in a dual-comb mode over a dozen hours.

METHODS

Generation of the dual-comb source

The experimental setup of our SCDC laser is shown in Fig. 1(a). The all-fiber ring cavity is approximately 1.4 m long, where the dual comb pulses share a common path while propagating in the same direction. Because the cavity is partially birefringent, the nearly orthogonally polarized pulses will travel at two different group velocities, and hence possess slightly mismatched repetition rates.

The ring cavity includes a 26 cm long piece of an erbium-doped fiber (EDF, Er150) forward-pumped by a 980 nm pump diode. To enable passive mode-locking, we use a graphene/poly(methyl methacrylate) (PMMA)-based saturable absorber placed onto the facet of an angle-polished fiber connector.[35] At the heart of the cavity is a hybrid component [Tap/Isolator/wavelength division multiplexing (TIWDM)] ensuring unidirectional operation of the laser, which additionally serves as an output coupler for the two combs (10% coupling ratio) and a wavelength division multiplexing (WDM) device for the pump. The birefringence of the cavity is provided predominantly by an 18 cm long section of a 980 nm polarization-maintaining fiber (PM980), with a beat-length of ~2 mm, corresponding to an effective refractive index difference Δn_{eff} of $\sim 8 \times 10^{-4}$. To control the repetition rate difference and intracavity polarization state, the PM fiber is preceded by an in-line polarization controller (PC), whereas the rest of the cavity consists of an ordinary single-mode 1550 nm fiber (SMF-28e) (the agility of the repetition rate difference is discussed in supplementary material, Note 2). The net cavity dispersion is estimated to be -0.02 ps^2; thus, the laser operates in the anomalous dispersion regime. Dual-comb lasing requires slight adjustments of the PC and a sufficient level of optical power pumping the EDF ranging from 110 mW to 121.6 mW provided by the pumping diode with ~350 mW of electrical power consumption in the high-power range. Losses introduced by the TIWDM component from the pump input to the output were equal to 8.8%. Photographs of the system along with a more comprehensive description of the cavity components are provided in the supplementary material.

Multiheterodyne beating

To enable multiheterodyne beating on a photodetector and thus an observation of dual-comb interferograms, the two combs available at the tap of the output coupler need to be guided through a birefringent optical element. We use a polarizing beam splitter (PBS)

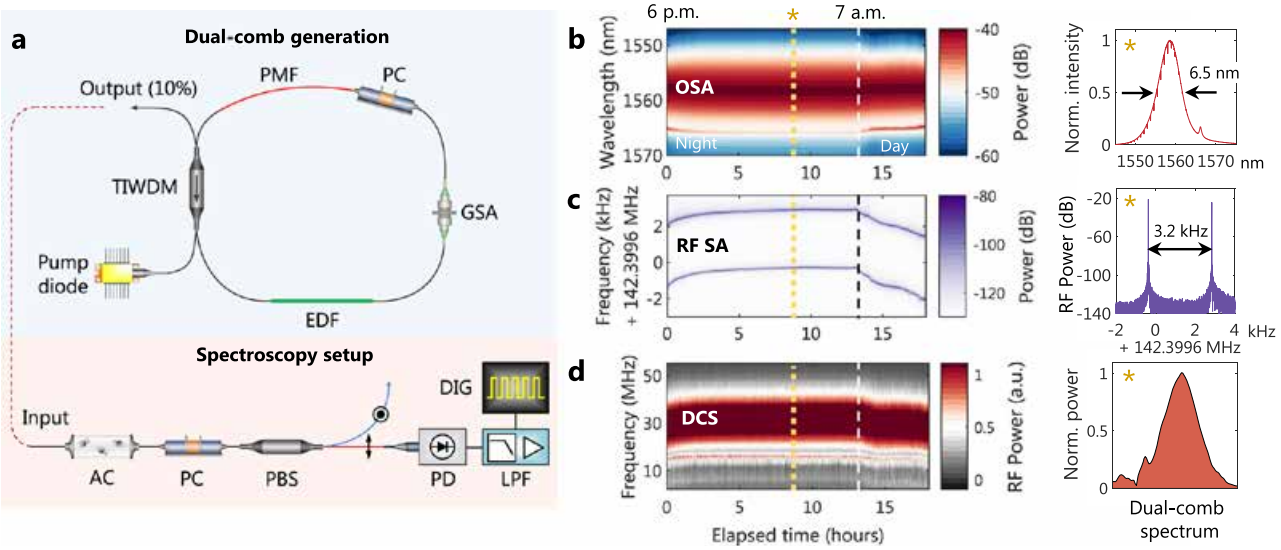

FIG. 1. Experimental setup for performing dual-comb spectroscopy together with long-term stability of the system. (a) The experimental setup consists of a dual-comb generation block (blue) and spectroscopy setup (orange panel). The dual-comb generation setup includes a polarization insensitive hybrid Tap/Isolator/WDM component (TIWDM), followed by a gain-providing low dispersion erbium-doped fiber (EDF) forward-pumped by a 980 nm pump diode. Passive mode-locking is enabled by a graphene-based saturable absorber (GSA), while the birefringence of the cavity is enhanced by a 980 nm polarization-maintaining fiber (PMF) preceded by an in-line PC. In the dual-comb spectroscopy setup, the output of the laser feeds a 10-Torr hydrogen cyanide absorption cell (AC). To maximize the heterodyne efficiency on the extended InGaAs photodetector, we use a PC and a polarizing beam splitter (PBS); however, dual-comb interferograms become detectable even after guiding the combs through a piece of the PM fiber. (b) Characterization of the optical spectrum over 18 h of uninterrupted operation. (c) Characterization of the dual-comb RF intermode beat notes. (d) Dual-comb spectrum retrieved from digitized interferograms plotted in the linear scale. The dashed line marked with an asterisk indicates the time instant at which we generated the cross section plots visible on the right, while that starting at 7 a.m. indicates the beginning of an increased system drift.

preceded by a PC adjusted to maximize the heterodyne efficiency and hence the strength of the DCS interferogram, albeit a piece of the PM fiber has shown to serve for this purpose as well yet with sub-optimal performance. In principle, the second (s-polarized) output of the PBS in our setup can be used for concurrent reference spectrum measurement, which is particularly desired for spectroscopy of broadband molecular absorbers. The optical power available on the photodetector was approximately 900 μW, yielding a millivolt-level RF electrical signal low-pass-filtered to 70 MHz and amplified by a low noise amplifier. To record a stream of DCS interferograms, we use an 8-bit oscilloscope in high-resolution (oversampling) mode with 11 effective number of bits (ENOB). To simplify the setup, we use a symmetric (collinear) configuration with a single photodetector, where both combs interrogate the sample [absorption cell (AC)] which is justified by the smooth shape of the optical soliton spectra for synthetic baseline fitting[40] and negligible frequency difference compared to the molecular linewidths probed here (see supplementary material, Note 3).

RESULTS

Stability of the dual-comb laser

One of the main prerequisites for widespread adoption of SCDC lasers outside the laboratory is the demonstration of their ability to sustain in dual-comb lasing mode over long time scales. To date, however, stability tests have been performed in intervals ranging from seconds to minutes, which left the question of their long-term operation feasibility unanswered. Initially, we encountered major issues with the reliability of the laser, but those were significantly minimized after we replaced the birefringent part of the ring. We observed that by using a PM fiber optimized for 980 nm (Panda PM 980) with a beat length reduced by 50% compared to PM1550, we can reach a kilohertz-range repetition rate difference with a considerable improvement in long-term stability of the dual-comb source. Figures 1(a)–1(c) plot the optical spectrum, the electrical intermode beat note spectrum, and the radio frequency dual-comb spectrum, respectively, measured in an overnight test lasting for 18 h and displayed in a waterfall form. During that time, the laser was left completely free-running, without active thermal stabilization and directly exposed to environmental mechanical and thermal fluctuations. For the first 5 h after dusk, the laser was reaching a steady state related to a temperature change in the laboratory, after which it operated with a negligible drift until morning (7 a.m.). With the morning start of the heating system and routine laboratory activities involving slight mechanical perturbations of the table, a slow drift of the repetition rates and optical spectrum can be observed, albeit the dual-comb operation was sustained until the end of the test interrupted on demand. The shared-cavity configuration ensured that the way the repetition rates evolved throughout the measurement was highly correlated, thus yielding high mutual stability. The side panels of Figs. 1(a) and 1(b) show a cross section of the spectral maps after 9 h with a smooth 6.5 nm wide soliton optical spectrum mapped to the radio frequency domain with a repetition rate difference of ~3.2 kHz.

Spectral characteristics

A major advantage of employing polarization multiplexing in the cavity for dual-comb generation is an excellent spectral overlap between the smooth soliton spectra provided intrinsically by the laser.[41] Figure 2 plots the polarization-resolved optical spectra centered around ~1560 nm measured with a resolution of 50 pm using an optical spectrum analyzer together with those retrieved from the radio-frequency interferograms. Due to different losses experienced in the ring cavity, the two polarizations slightly differ in peak intensities (~15%), and in center wavelengths, yet by only ~1 nm, as shown in Figs. 2(a) and 2(b). Both effects, however, have almost no effect on the RF dual-comb spectrum which is the product of the comb teeth intensities rather than the sum. The overall shape of the optical spectrum resembles that of soliton lasers operating in the negative dispersion regime. The characteristic peak-dip sideband located more than a terahertz from the carrier manifests the coherent energy exchange between the orthogonally polarized components of the generated vector solitons.[42] Figure 2(c) illustrates a notable discrepancy in the polarization extinction ratio (PER) of the individual combs. The lower repetition rate RF beat note corresponding to the comb centered around a shorter wavelength has a well-defined polarization with a PER of ~30 dB, as opposed to the higher repetition rate comb shifted toward longer wavelengths with a PER of ~10 dB. By adjusting the PC before the PBS, we maximize the strength of the beating signal, which we coherently average and Fourier-transform, as plotted in panels (d) and (e) of Fig. 2 to illustrate the aliasing-free mapping of the optical to radio-frequency domains for comparative purposes. Figure 2(f) plots the clean temporal structure of the DCS signal.

Linewidth measurements

For the demanding application of free-running Doppler-limited spectroscopy, it is of utmost importance to carefully characterize the relative and absolute stability of the comb teeth. For this purpose, we optically beat a narrow-linewidth (~200 kHz) 1560 nm continuous wave (CW) laser with two comb teeth, one from each comb,[30] and record the signal over 10 ms. Figure 3(a) shows the spectrogram of the low-pass filtered beating signal with visible frequency oscillations of the two RF lines, albeit with a high degree of visual similarity. By mixing the RF lines through a nonlinear operation on the signal (see the supplementary material), we observe that most of these fluctuations are common and yield a straight-line differential frequency component in Fig. 3(b). To fully characterize the efficacy of common phase noise suppression, we

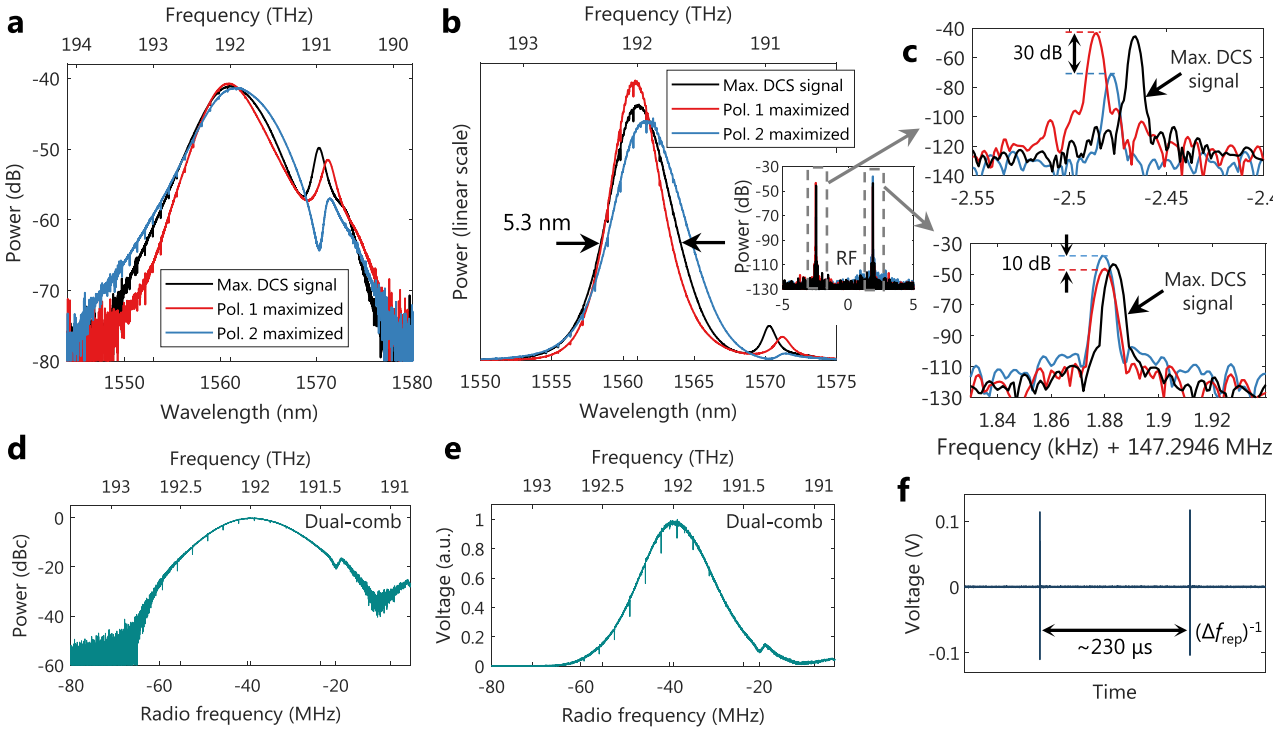

FIG. 2. Optical and radio frequency spectra of the dual-comb laser after passing through a 10-Torr hydrogen cyanide absorption cell measured at different positions of the PC before the PBS [maximum RF beat note power for both polarizations (Pol. 1/Pol. 2) and maximum power of the DCS signal]. (a) Optical spectrum in a logarithmic scale measured with a resolution of 50 pm. (b) Optical spectrum in a linear intensity scale showing the smooth soliton shape and excellent spectral overlap. The detuning of the central wavelengths is ~1 nm. (c) Radio frequency intermode beat notes corresponding to the optical spectra in (a) and (b) at different settings of the PC. The lower-repetition rate beat note corresponds to the shorter-wave-centered comb with a higher polarization extinction ratio (PER) of ~30 dB compared to the longer-wavelength-centered with a PER of ~10 dB. (d) Optical spectrum in a logarithmic scale retrieved from dual-comb interferograms acquired over 200 ms. (e) The same plot as (d) but in a linear intensity scale. (f) Clean temporal structure of the dual-comb signal with a single burst per $1/\Delta f_{rep}$.

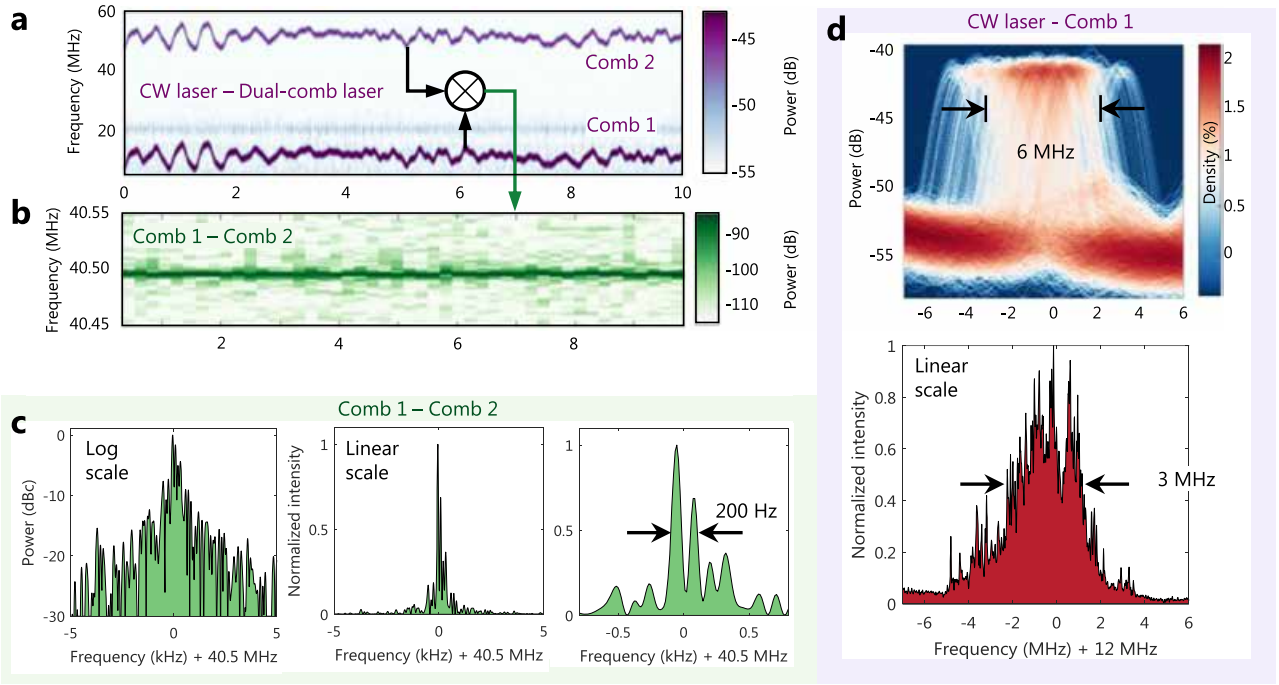

FIG. 3. Experiment with a narrow-line continuous wave (CW) laser to characterize the absolute stability and mutual coherence of the combs. (a) Spectrogram of the heterodyne signal between the CW laser and two comb teeth, one from each comb. The high visual similarity of the traces indicates a high degree of coherence. (b) Spectrogram of the mixing between the two comb teeth showing a straight line almost free of frequency fluctuations. (c) Fourier transform of the intertooth mixing signal plotted in different scales revealing the relative linewidth of 200 Hz within a 100 Hz resolution bandwidth, which is an order of magnitude lower than the repetition rate difference of 4.655 kHz as required for the computational correction. (d) Beat note of one comb line and the CW laser plotted in the persistence spectrum with a logarithmic scale, and the conventional frequency spectrum form in a linear intensity scale. In the persistence spectrum measured with a 1.56 MHz resolution bandwidth, it is clearly visible that for a majority of time, the beat note stays in a 6 MHz bandwidth with very sporadic excursions up to <10 MHz. The Fourier-transform-based analysis (which is not well suited for nonstationary signals) provides a linewidth estimate on the order of 3 MHz.

calculate the Fourier transform of the time-domain intercomb mixing signal and measure a relative linewidth between the combs of 200 Hz. This is several orders of magnitude lower compared to the absolute linewidth (coarsely estimated to be 3 MHz) and proves that the laser shows mutual coherence on time scales much greater than $1/\Delta f_r$, as required by the computational correction. Such narrow free-running relative linewidths have been previously reported only in dual-wavelength configurations[22–26] and may suggest that the large repetition rate difference of several kilohertz is not necessary. Unfortunately, the opposite is true. We estimated that 80% of the relative beat note power is carried in a 3 kHz bandwidth over 10 ms, and 90% in 6.8 kHz (see supplementary material, Note 4). Consequently, to resolve extremely narrow Doppler-limited features, we mismatch the repetition rates wih ~4.65 kHz to optimally use the available alias-free RF and optical bandwidths.

To measure the optical (absolute) linewidth of the comb teeth, we analyzed the lower-frequency beat note in Fig. 3(a) originating from optical beating between the CW laser and a comb tooth close to the RF carrier frequency. Due to its high nonstationarity and rapid frequency fluctuations, we analyzed the beat note in two ways to better visualize the sporadic excursions over a wider frequency range. Figure 3(d) plots a beat note persistence spectrum, where most of the fluctuations reside in a 6 MHz bandwidth with maximal drifts not exceeding 5 MHz from the center. The conventional frequency spectrum plotted in a linear intensity scale provides an even more optimistic estimate of ~3 MHz. We should underline here that the retrieved value is of course not as accurate as that measured in an experiment with a hertz-stabilized frequency comb.[43] Instead, it provides an upper bound due to the convolution between the profiles of the submegahertz-wide CW laser and the comb line. Even though the true comb linewidth is consequently overestimated, it is almost a 100 times narrower compared to the room temperature Doppler linewidths of typical molecular absorbers with a low molecular weight, such as $H^{13}C^{14}N$ investigated here.

Dual-comb interferograms and phase correction

Using a fast digital oscilloscope, we acquired a stream of dual-comb-interferograms with an RF repetition rate of $\Delta f_{rep} = 4.655$ kHz sampled at 400 MS/s. The temporal structure of a single frame (coherently averaged) is shown in Fig. 4(a) with a clearly visible extremely short zero path difference (ZPD) burst lasting for approximately 100 ns, which is a time-magnified (compression factor $m = 31\,642$) interval of 3.16 ps related to the cross-correlation between the electric fields of the two combs in the optical domain. It is surrounded by a periodic interferometric modulation induced

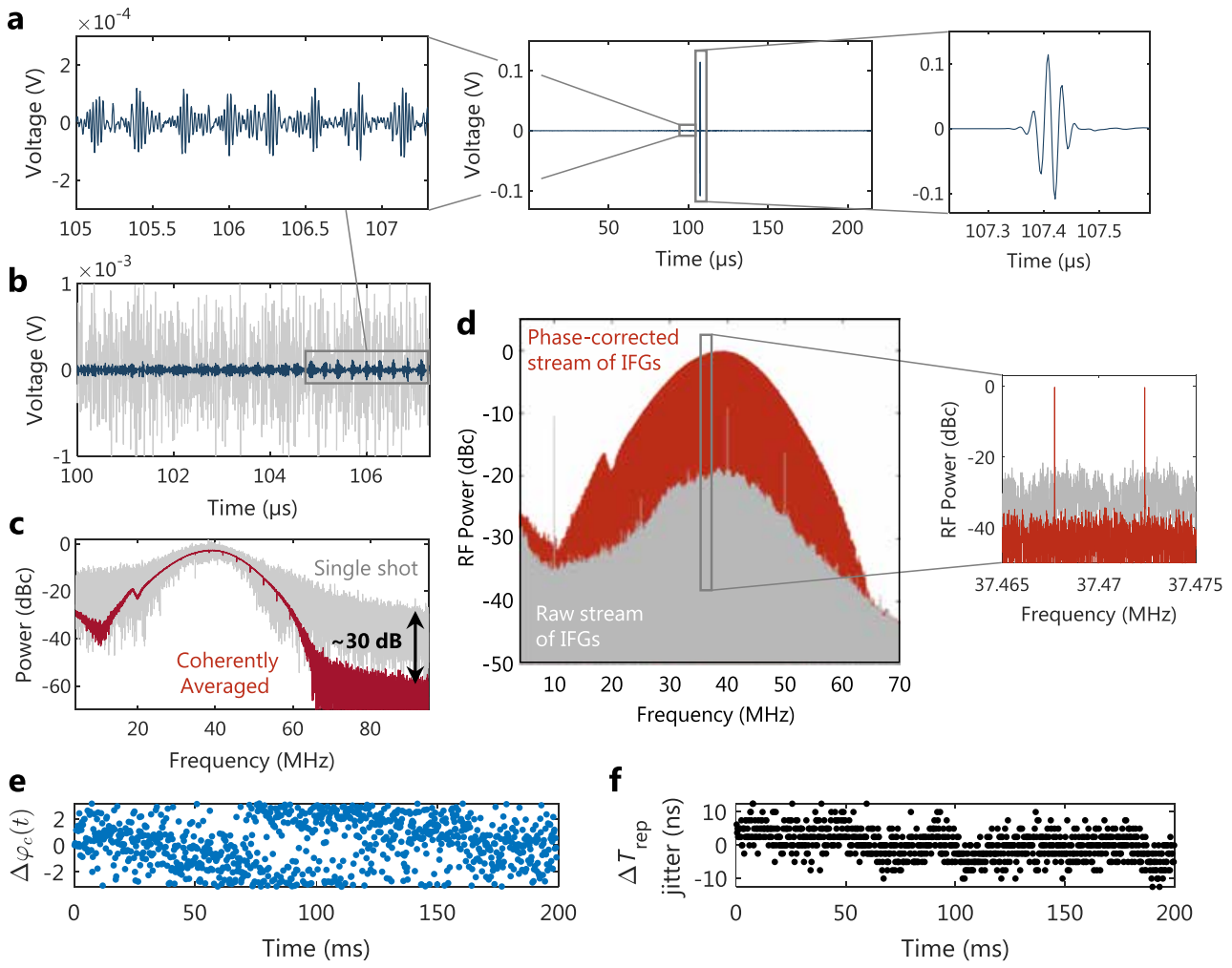

FIG. 4. Dual-comb interferograms and their Fourier transforms. (a) Time-domain dual-comb interferogram after computationally enabled coherent averaging of 926 interferograms (~200 ms). (b) Zoomed in interferometric modulation induced by the free-induction decay of HCN molecules plotted atop of a single-shot trace. (c) Power spectra of the single-shot and coherently averaged interferograms. (d) Tooth-resolved RF spectra of the corrected and raw stream of interferograms. (e) Phase increments between the consecutive interferogram frames. (f) Repetition rate difference jitter. 10 ns of the interferogram duration jitter correspond to ~316 fs of laboratory time.

by the molecular lines of $H^{13}C^{14}N$ known as the free-induction decay, which can be clearly identified here when the temporal signal is averaged. Figure 4(b) shows that in a single-shot mode, these weak features are buried in noise; hence, they necessitate prolonged coherent averaging for noise suppression and reliable spectroscopic assessments. In Fig. 4(c), one can see that the power spectrum of a single-shot trace shows a large variance with a poor ~10 dB spectral signal-to-noise ratio (SNR) and does not resemble the expected smooth soliton shape. This changes drastically for the coherently average trace, where regularly spaced narrow lines of hydrogen cyanide become noticeable. The noise floor in the frequency spectrum lowers by approximately 30 dB, being consistent with the number of averaged interferogram frames (see supplementary material, Note 5 for evaluation of the coherent averaging efficacy).

To perform the time-domain averaging demonstrated in the panels of Fig. 4, we propose a novel computational phase retrieval and a correction algorithm suitable for fast coherent averaging of DCS data. Basically, the RF comb in DCS shows two kinds of instabilities: that of the repetition rate and that of the frequency offset, which smear out the discrete character of RF lines. The algorithm used here corrects for both sources of instabilities in an all-computational way relying only on digitized DCS data from a single detector, which is in stark contrast to the widely adapted CW-laser referencing schemes. Without averaging, the Fourier spectrum of a stream of DC interferograms [Fig. 4(d)] turns into a featureless blob with some spurious RF lines originating from harmonics and subharmonics of the digitizer clock. The phase and timing manipulation restores the initially corrupted shape of the spectrum with a Fourier-limited linewidth and a suppression of the

spurious noncomb lines. A detailed description of the procedure is provided in Methods, but in short, we took a radical departure from the cross-ambiguity,[38,44] Fourier-based phase retrieval or Kalman filter[37,45] paradigms, which hampered the speed of computational correction algorithms. Our time-domain-only solution relies on a constant fraction discriminator (CFD) to track the arrival times of consecutive centerbursts and hence estimate variations in the repetition rate difference (timing jitter), followed by tracking carrier phase and frequency increments between consecutive interferogram frames, results of which are plotted here in Figs. 4(e) and 4(f). After frame-by-frame resampling (equivalent to adaptive sampling proposed by Ideguchi *et al.*[43]) followed by phase correction, we obtain a carrier-envelope-offset-free stream of interferograms possible to process in two ways. In the first, they can be coherently coadded to produce a single time-domain trace with an extremely high dynamic range (see supplementary material, Note 5). The second approach is to stitch all interferograms just like they were produced by an intrinsically phase-stable dual-comb spectrometer[46] and calculate a tooth-resolved RF spectrum with a linewidth limited by the acquisition time.

Allan deviation analysis

While the phase correction allows us to correct for residual phase excursions throughout the measurement, it is always accompanied by the risk that some undesired modulations introduced by the procedure may corrupt the amplitude. We performed an Allan deviation analysis of amplitude on two RF beat notes with different strengths and distances from the center frequency located around 20 MHz and 40 MHz, respectively, as shown in Fig. 5. The dashed lines correspond to uncorrected data, whereas the thick solid lines correspond to data after phase correction. The gain of the phase correction becomes noticeable above 10 ms (~47 interferograms), when the amplitude uncertainty of uncorrected data starts to deviate from a decreasing trend. The weak beat note (20 MHz) yields an SNR close to 90 after 100 ms of coherent integration, while the strong (40 MHz) one reaches a per mille precision regime, which would not have been possible without the digital correction. The nearly 10-fold discrepancy in SNRs between the beat notes is responsible for an increased standard deviation of the spectroscopic fit close to the edges of the dual-comb spectrum.

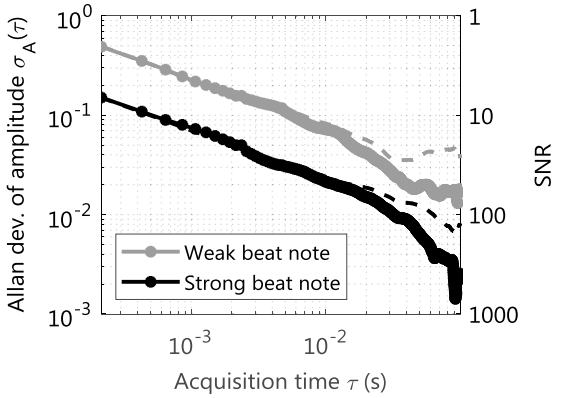

FIG. 5. Allan deviation of the (normalized) beat note amplitude for two different RF lines with (solid line) and without (dashed line) the phase correction.

Doppler-limited spectroscopy of hydrogen cyanide

Finally, to unequivocally prove the high resolution capabilities of our system and the efficacy of the correction procedure, we measure a molecular sample of hydrogen cyanide ($H^{13}C^{14}N$) at room temperature (22 °C) and a low pressure of 10 Torr. In this regime, absorption linewidths are predominantly limited by Doppler broadening. Around 1560 nm, the Doppler half width at half maximum (HWHM) is assumed to be constant, equal to $\alpha_D = 225(1)$ MHz, which combined with Lorentzian pressure-broadening coefficients as low as ~10 MHz/Torr renders relatively narrow lines with FWHM Voigt profile linewidths below 600 MHz. In the dual-comb spectrum, it corresponds to approximately 4 lines in a logarithmic absorbance scale, and a bit more in linear transmission.

Because our system is left completely free-running and it is intended to be used without any additional optical components but the oscillator itself, we take advantage of the sharp HCN lines with well-defined frequencies, to anchor the optical frequency axis (*P*20 transition is used here) for spectroscopic assessments. We acquire DCS data in 200 ms (limited by the digitizer) and process it in the aforementioned coherently averaged single-frame mode, where a 85 930-point Fourier transform yields discrete points corresponding exactly to the individual RF comb teeth without any line shape influence. The computational correction of the DCS data on a Core-i7 PC computer with 32 GB of memory takes approximately 24 s, yet no significant efforts were put on optimizing the performance of the code written in a high-level Matlab environment. It is, however, real-time compatible thanks to its frame-by-frame architecture, and it should be possible to implement it in a hardware platform such as field-programmable gate array.

To calculate the optical transmission, we leverage the smooth shape of the spectrum and fit a synthetic baseline[40] using a robust parabolic regression method to serve as a zero-gas measurement for spectral deconvolution. We analyze the amplitude rather than power spectra to calculate the transmission because both combs interrogate the sample, as opposed to the widely used dispersive configuration.[11] Figure 6(a) plots the results of the DCS-based optical transmission measurement together with a multiline Voigt profile fit based on parameters in Ref. 47 (see Methods for details). Since no comprehensive spectroscopic models are available for this hydrogen cyanide isotope ($H^{13}C^{14}N$), to prove the validity of our results, we performed an additional tunable diode laser absorption spectroscopy (TDLAS) experiment using the same cell, wherein the frequency of the high-fidelity tunable CW laser was swept over ~10 s and the intensity was measured using the same photodetector and oscilloscope. For optical axis calibration, this time we used two absorption lines of the *P* branch—*P*24 and *P*20 with vacuum frequencies and pressure shift coefficients derived from the literature.[47] Both transmission spectra are plotted in mirrored panels for comparative purposes and show a high degree of mutual similarity.

The quality of the measured DCS data can be accurately evaluated in spectroscopic terms by analyzing the three lines of the *P* branch captured in the spectrum that have been modeled using quantum chemistry methods[48] with confirmed experimental

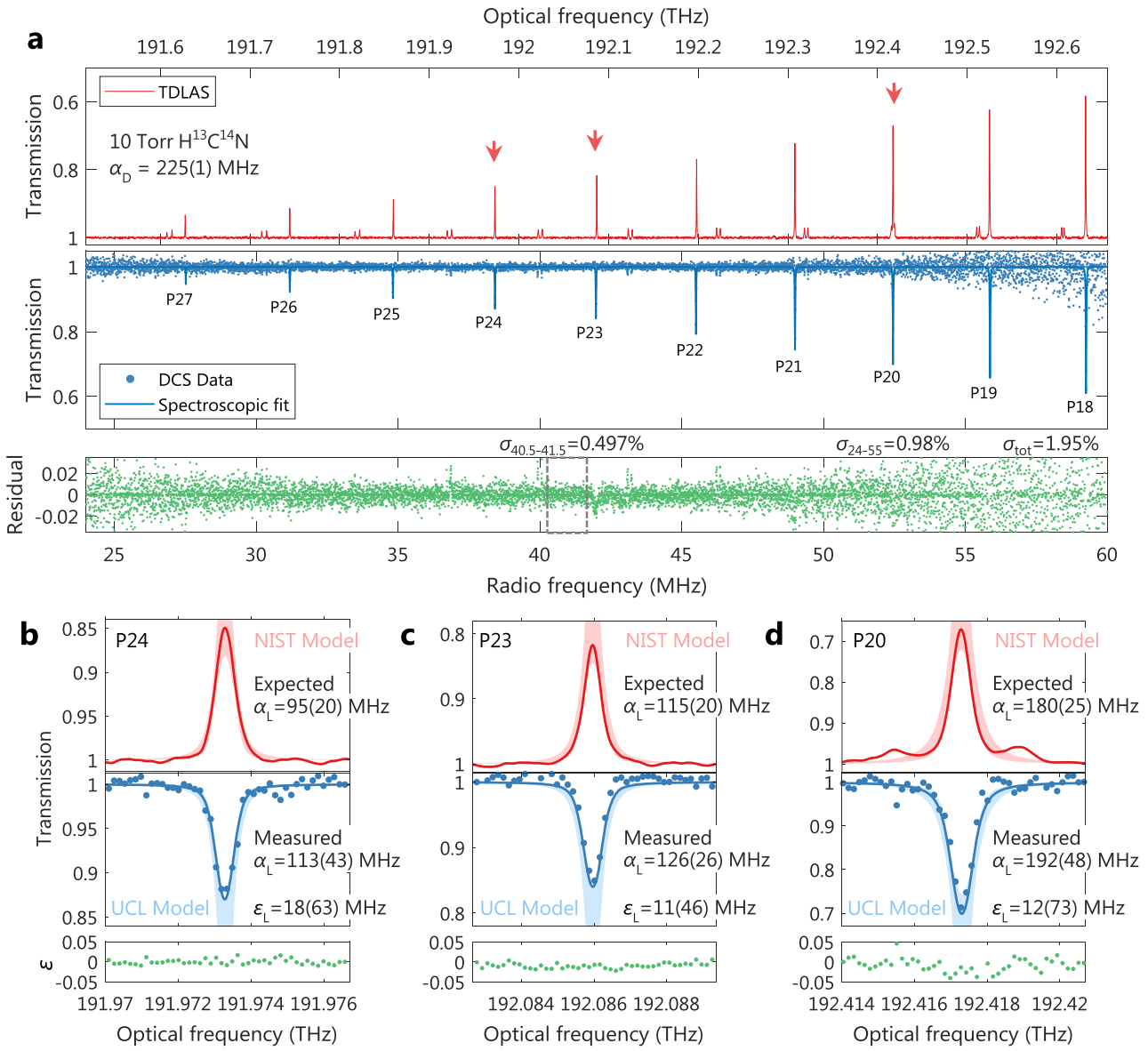

FIG. 6. Illustration of the quality of the computationally corrected DCS spectrum of $H^{13}C^{14}N$ at 10 Torr obtained using the dual-comb laser in free-running mode within 200 ms. (a) DCS linear transmission spectra (bottom) plotted together with tunable diode laser absorption spectroscopy (TDLAS, top) showing a high degree of mutual similarity. A multiline Voigt fit to the dominant transitions in the $2\nu_3$ band was obtained from the scatter-point DCS data, while weak interfering hot bands were left unmodeled. The residual calculated from the difference between the DCS data and the fit has a standard deviation of 0.98% in a ~1 THz bandwidth, and 1.95% in total. The peak spectroscopic SNR available in a 30 GHz optical bandwidth (40.5–41.5 MHz in the RF) exceeds 200. (b) *P*24 line, (c) *P*23 line, and (d) *P*20 line measured with the dual-comb spectrometer (scattered points) together with a Voigt fit solid line (bottom panel) compared with a tunable laser scan (top panel) and two spectroscopic models. The measured Lorentzian widths are in good agreement with the literature data, and the difference between the expected and measured values lies within the uncertainty of the model. These lines have some degree of weak hot-band interference which may corrupt the fits. Particularly, the *P*20 line is surrounded by two unmodeled lines constituting a pronounced oscillatory shape of the residual. Additional weak oscillations on the wings of the absorption lines are caused by Fabry-Pérot etalons from the gas cell.

validation.[30,47] In our dataset, we can only model lines *P*24, *P*23, and *P*20 (the only ones available with pressure broadening coefficients) and denote the quantum chemistry-based (ExoMol database[48]) simulation as UCL (University College London), whereas the experimentally obtained line intensities were used in the NIST (National Institute of Standards and Technology) model.[30] The reason for the simultaneous use of both is that discrepancies in line intensities as large as 11% have been reported,[30] and the exact values may still require further experimental verification. The shaded area in Figs. 6(b) and 6(c), and c correspond to 2σ (95%) confidence

intervals associated with combined uncertainties of the broadening coefficients, line intensities, and gas pressure (see Methods). In addition, based on the Voigt fits, we compare the fitted Lorentzian half widths α_L for the three available lines with pressure broadening coefficients reported in Ref. 47.

Overall, we obtain excellent agreement between the Voigt fits and DCS data (also including the lines without a spectroscopic model). Peak intensities of the lines follow the same increasing trend as that in the TDLAS measurement and reach values different from the TDLAS measurement by ~2% of the transmission scale in the worst cases, possibly attributable to slight nonlinearities of the photodetector causing a difference in the response at different optical power levels. An alternative explanation involves optical fringe noise arising due to parasitic reflections at different optical interfaces in the system. The modeled lines *P*24 and *P*23 generally possess lower oscillations on the wings compared to *P*20 due to their much weaker hot-band interference. The presence of those weak unmodeled transitions adjacent to strong lines necessitates to limit the range of data around the peaks for the fitting routine[47] (see the supplementary material) and contributes to sharp dips in the residual due to their exclusion from the spectroscopic model. The fitted Voigt profiles are consistent with the theoretical UCL and NIST models and lie within their 2σ confidence intervals. The same is true with respect to the fitted Lorentzian linewidths, which match the literature values within uncertainties associated with them.

This proves that such a simple laser combined with the computational algorithm renders quality spectra in the Doppler-limited resolution range. Within 200 ms, we achieve better than 1% absorption precision in a ~1 THz optical bandwidth, and less than 2% over the full span of ~1.14 THz width, based on the fit residual. It corresponds to noise equivalent absorptions (NEAs) of 4.4×10^{-3} $Hz^{-1/2}$ and 8.7×10^{-3} $Hz^{-1/2}$, respectively, whereas the figure-of-merit (FOM) defined as the SNR at 1 s of averaging (NEA^{-1}) multiplied by the number of resolved lines M in a given bandwidth[49] yields 1.5×10^6 $Hz^{1/2}$ in 1 THz when $M = 6660$, and 8.9×10^5 $Hz^{1/2}$ in the full 1.14 THz window when $M = 7734$. The maximum spectroscopic SNR obtainable with our system within 0.2 s exceeds 200 in a 30 GHz optical span around 192.05 THz.

As a final demonstration of the computationally enabled spectrometer performance, we plot an RF tooth-resolved dual-comb spectrum covering ~1.7 THz mapped on more than 11 000 lines. This is the largest number of self-corrected lines of a free-running dual-comb system reported to date (i.e., without using any CW lasers, $f - 2f$ interferometry, and additional optoelectronic components[43]). Figure 7 plots the spectrum with different magnification factors of the frequency axis and confirms that even components located thousands of lines away from the carrier have a comb structure without any increase in the linewidth or appearance of a pronounced noise pedestal.

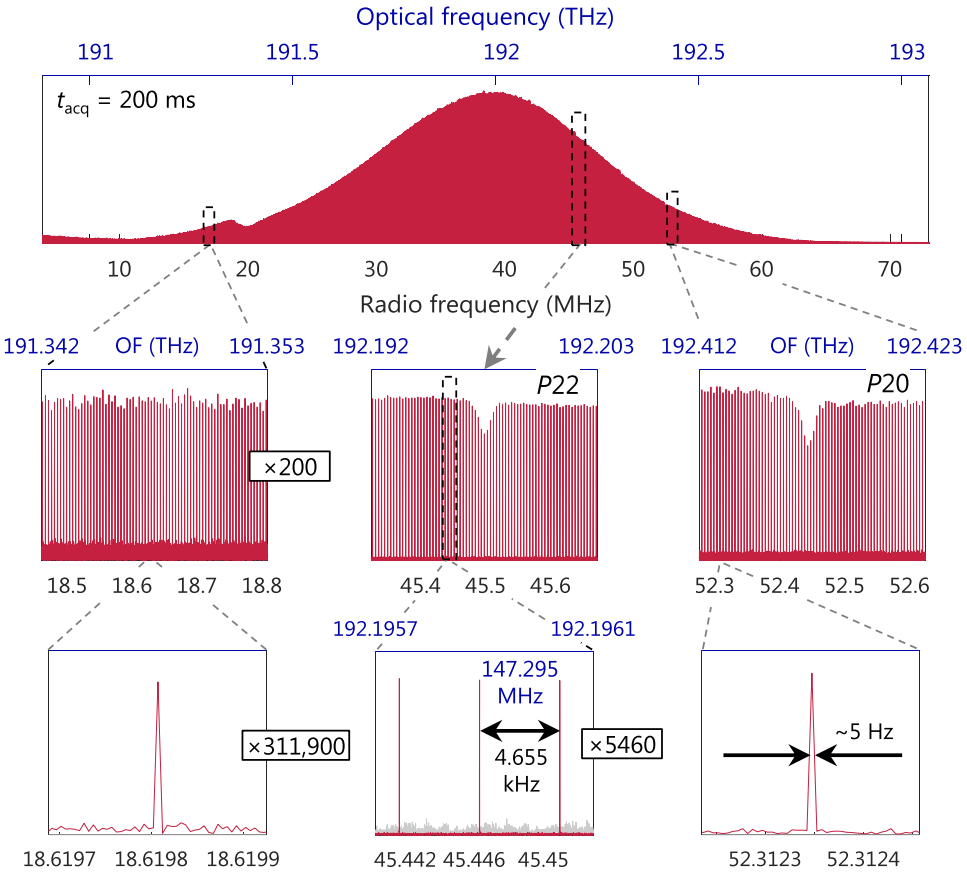

FIG. 7. Computationally corrected dual-comb amplitude spectrum in a linear scale covering 1.7 THz in the optical domain with resolved 11 000 RF comb lines plotted with different magnification factors on the frequency axis. The central panels include two transitions of the $H^{13}C^{14}N$ *P* branch: *P*22 and *P*20 with different levels of signal-to-noise ratios. The bottom panel with three comb teeth includes additionally the spectrum without phase correction (gray blurred trace) with spectroscopic information dispersed over a large RF bandwidth. The 5 Hz corrected beat note linewidth is an upper limit given by the acquisition time.

CONCLUSIONS

Our demonstration of free-running high-resolution spectroscopy using an ultrasimple, all-fiber single-cavity dual-comb laser (AFSCDCL) relying on polarization multiplexing inside a birefringent cavity bodes for a wide range of possible applications in the laboratory and industrial environment. Our low-drive-power and cost-effective dual-comb spectrometer with an easily tailorable repetition rate difference accompanied by a high repetition rate exceeding 140 MHz permits a further extension of the optical bandwidth without optical aliasing in DCS. We prove that operation of an AFSCDCL on a dozen-hour time scale is possible, albeit without any indication that the ultimate limit is reached. By merging the simple cavity design utilizing just a few basic fiber components with our novel all-computational phase retrieval and correction algorithm, we can effectively suppress residual phase fluctuations of dual-comb interferograms, thus rendering high-quality molecular dual-comb spectra with tooth-resolved lines, subpercentage transmittance precision in a terahertz bandwidth measured in a fraction of a second, and corrected within a user-acceptable time of less than half a minute. The processing speed, however, is not a limitation *per se* and can be easily improved by implementing the algorithm in a hardware platform or by lowering the computational payload through an external quadrature demodulator. The excellent agreement between the measured spectroscopic data in the Doppler-limited regime and spectroscopic models together with a narrow-linewidth tunable diode laser scan proves that computationally corrected free-running spectrometers are suitable for high-resolution spectroscopy applications, and that more than 10 000 teeth in the dual-comb spectrum can be corrected without noticeable degradation of lines away from the carrier. Here, the gain of computational coherent averaging reached 99.3% of the theoretical. In principle, the algorithm demonstrated here can also be used for novel emerging single-cavity DCS platforms based on bidirectionally[13] or orthogonally locked[50] microresonator combs, whose size, monolithic integration capability, and high repetition rates make them a choice of preference for compact dual-comb spectrometers of liquid and solid samples.

Although our free-running dual-comb fiber source will never reach the precision and accuracy of the highly stabilized and absolutely referenced frequency combs with enhancement cavities,[51] optical frequency fluctuations occurring on typical measurement time scales do not preclude measurements of high-quality low-pressure molecular spectra. With future developments involving use of an ultralow-noise pump diode and active environmental stabilization of the cavity, we anticipate further improvements of the optical bandwidth and system stability. Most importantly, to exploit the full spectroscopic potential of the developed AFSCDCL enhanced by the flexible coherent averaging procedure, we will focus on shifting the comb wavelengths through nonlinear conversion to other spectral regions such as the mid- or far-infrared.

SUPPLEMENTARY MATERIAL

See the supplementary material for the complete description of the setup, and additional data and methods that support the main conclusions in the paper.

ACKNOWLEDGMENTS

We warmly thank Dr. Adam Fleisher of the NIST for useful comments regarding the uncertainty budget of spectroscopy of HCN, and Rohde & Schwarz Poland for lending us the real-time radio-frequency analyzer. This work was partially supported by the National Science Centre (NCN, Poland) under Grant No. UMO-2014/13/D/ST7/02143; the Statutory Funds of the Chair of EM Field Theory, Electronic Circuits and Optoelectronics (Mloda Kadra No. 0402/0157/18); and by the Research Foundation Flanders (FWO) under Grant No. EOS 30467715. Ł. A. Sterczewski acknowledges support from the Foundation for Polish Science within the START Program (START 085.2018).

REFERENCES

[1] N. Picqué and T. W. Hänsch, Nat. Photonics **13**, 146 (2019).
[2] T. W. Hänsch, Ann. Phys. **15**, 627 (2006).
[3] D. J. Jones, S. A. Diddams, J. K. Ranka, A. Stentz, R. S. Windeler, J. L. Hall, and S. T. Cundiff, Science **288**, 635 (2000).
[4] S. A. Diddams, D. J. Jones, J. Ye, S. T. Cundiff, J. L. Hall, J. K. Ranka, R. S. Windeler, R. Holzwarth, T. Udem, and T. Hänsch, Phys. Rev. Lett. **84**, 5102 (2000).
[5] I. Coddington, W. C. Swann, and N. R. Newbury, Phys. Rev. Lett. **100**, 013902 (2008).
[6] R. Holzwarth, T. Udem, T. W. Hänsch, J. Knight, W. Wadsworth, and P. S. J. Russell, Phys. Rev. Lett. **85**, 2264 (2000).
[7] T. Udem, R. Holzwarth, and T. W. Hänsch, Nature **416**, 233 (2002).
[8] C.-H. Li, A. J. Benedick, P. Fendel, A. G. Glenday, F. X. Kärtner, D. F. Phillips, D. Sasselov, A. Szentgyorgyi, and R. L. Walsworth, Nature **452**, 610 (2008).
[9] D. van der Weide and F. Keilmann, *Coherent Periodically Pulsed Radiation Spectrometer* (Google Patents, 1998).
[10] F. Keilmann, C. Gohle, and R. Holzwarth, Opt. Lett. **29**, 1542 (2004).
[11] I. Coddington, N. Newbury, and W. Swann, Optica **3**, 414 (2016).
[12] M.-G. Suh, Q.-F. Yang, K. Y. Yang, X. Yi, and K. J. Vahala, Science **354**, 600 (2016).
[13] Q.-F. Yang, X. Yi, K. Y. Yang, and K. Vahala, Nat. Photonics **11**, 560 (2017).
[14] B. Stern, X. Ji, Y. Okawachi, A. L. Gaeta, and M. Lipson, Nature **562**, 401 (2018).
[15] G. Villares, A. Hugi, S. Blaser, and J. Faist, Nat. Commun. **5**, 5192 (2014).
[16] J. Westberg, L. Sterczewski, and G. Wysocki, Appl. Phys. Lett. **110**, 141108 (2017).
[17] L. A. Sterczewski, J. Westberg, M. Bagheri, C. Frez, I. Vurgaftman, C. L. Canedy, W. W. Bewley, C. D. Merritt, C. S. Kim, M. Kim, J. R. Meyer, and G. Wysocki, Opt. Lett. **44**, 2113 (2019).
[18] K. Kieu and M. Mansuripur, Opt. Lett. **33**, 64 (2008).
[19] S. Mehravar, R. A. Norwood, N. Peyghambarian, and K. Kieu, Appl. Phys. Lett. **108**, 231104 (2016).
[20] M. I. Kayes, N. Abdukerim, A. Rekik, and M. Rochette, Opt. Lett. **43**, 5809 (2018).
[21] V. Mamidala, R. Woodward, Y. Yang, H. Liu, and K. K. Chow, Opt. Express **22**, 4539 (2014).
[22] X. Zhao, G. Hu, B. Zhao, C. Li, Y. Pan, Y. Liu, T. Yasui, and Z. Zheng, Opt. Express **24**, 21833 (2016).
[23] K. Lau, M. A. Bakar, F. Muhammad, A. Latif, M. Omar, Z. Yusoff, and M. Mahdi, Opt. Express **26**, 12790 (2018).
[24] R. Li, H. Shi, H. Tian, Y. Li, B. Liu, Y. Song, and M. Hu, Opt. Express **26**, 28302 (2018).
[25] C. Zeng, Y. D. Cui, and J. Guo, Opt. Commun. **347**, 44 (2015).
[26] R. Liao, Y. Song, W. Liu, H. Shi, L. Chai, and M. Hu, Opt. Express **26**, 11046 (2018).
[27] J. Fellinger, A. S. Mayer, G. Winkler, W. Grosinger, G.-W. Truong, S. Droste, C. Li, C. M. Heyl, C. M. Heyl, I. Hartl, and O. H. Heckl, Opt. Express **27**, 28062 (2019).

[28]Y. Liu, X. Zhao, G. Hu, C. Li, B. Zhao, and Z. Zheng, Opt. Express **24**, 21392 (2016).
[29]G. Millot, S. Pitois, M. Yan, T. Hovhannisyan, A. Bendahmane, T. W. Hänsch, and N. Picqué, Nat. Photonics **10**, 27 (2016).
[30]P. Guay, J. Genest, and A. J. Fleisher, Opt. Lett. **43**, 1407 (2018).
[31]S. M. Link, A. Klenner, M. Mangold, C. A. Zaugg, M. Golling, B. W. Tilma, and U. Keller, Opt. Express **23**, 5521 (2015).
[32]A. E. Akosman and M. Y. Sander, Opt. Express **25**, 18592 (2017).
[33]S. M. Link, D. J. Maas, D. Waldburger, and U. Keller, Science **356**, 1164 (2017).
[34]X. Zhao, T. Li, Y. Liu, Q. Li, and Z. Zheng, Photonics Res. **6**, 853 (2018).
[35]A. Krajewska, I. Pasternak, G. Sobon, J. Sotor, A. Przewloka, T. Ciuk, J. Sobieski, J. Grzonka, K. M. Abramski, and W. Strupinski, Appl. Phys. Lett. **110**, 041901 (2017).
[36]B. C. Smith, B. Lomsadze, and S. T. Cundiff, Opt. Express **26**, 12049 (2018).
[37]D. Burghoff, Y. Yang, and Q. Hu, Sci. Adv. **2**, e1601227 (2016).
[38]N. B. Hébert, J. Genest, J.-D. Deschênes, H. Bergeron, G. Y. Chen, C. Khurmi, and D. G. Lancaster, Opt. Express **25**, 8168 (2017).
[39]L. A. Sterczewski, J. Westberg, and G. Wysocki, Opt. Express **27**, 23875 (2019).
[40]X. Cui, C. Lengignon, W. Tao, W. Zhao, G. Wysocki, E. Fertein, C. Coeur, A. Cassez, L. Croize, W. Chen, Y. Wang, W. Zhang, X. Gao, W. Liu, Y. Zhang, and F. Dong, J. Quant. Spectrosc. Radiat. Transfer **113**, 1300 (2012).
[41]J. Nürnberg, C. G. E. Alfieri, Z. Chen, D. Waldburger, N. Picqué, and U. Keller, Opt. Express **27**, 3190 (2019).
[42]H. Zhang, D. Y. Tang, L. M. Zhao, and N. Xiang, Opt. Express **16**, 12618 (2008).
[43]T. Ideguchi, A. Poisson, G. Guelachvili, N. Picqué, and T. W. Hänsch, Nat. Commun. **5**, 3375 (2014).
[44]N. B. Hébert, V. Michaud-Belleau, J. Deschênes, and J. Genest, IEEE J. Quantum Electron. **55**, 1 (2019).
[45]D. Burghoff, N. Han, and J. H. Shin, Opt. Lett. **44**, 2966 (2019).
[46]Z. Chen, M. Yan, T. W. Hänsch, and N. Picqué, Nat. Commun. **9**, 3035 (2018).
[47]W. C. Swann and S. L. Gilbert, J. Opt. Soc. Am. B **22**, 1749 (2005).
[48]J. Tennyson, S. N. Yurchenko, A. F. Al-Refaie, E. J. Barton, K. L. Chubb, P. A. Coles, S. Diamantopoulou, M. N. Gorman, C. Hill, A. Z. Lam, L. Lodi, L. K. McKemmish, Y. Na, A. Owens, O. L. Polyansky, T. Rivlin, C. Sousa-Silva, D. S. Underwood, A. Yachmenev, and E. Zak, J. Mol. Spectrosc. **327**, 73 (2016).
[49]N. R. Newbury, I. Coddington, and W. Swann, Opt. Express **18**, 7929 (2010).
[50]C. Bao, P. Liao, A. Kordts, L. Zhang, A. Matsko, M. Karpov, M. H. P. Pfeiffer, G. Xie, Y. Cao, A. Almaiman, M. Tur, T. J. Kippenberg, and A. E. Willner, Opt. Lett. **44**, 1472 (2019).
[51]W. Zhang, X. Chen, X. Wu, Y. Li, and H. Wei, Photonics Res. **7**, 883 (2019).